

# Subtle cytotoxicity and genotoxicity differences in superparamagnetic iron oxide nanoparticles coated with various functional groups

Seong Cheol Hong<sup>1,\*</sup>Jong Ho Lee<sup>1,\*</sup>Jaewook Lee<sup>1</sup>Hyeon Yong Kim<sup>1</sup>Jung Youn Park<sup>2</sup>Johann Cho<sup>3</sup>Jaebeom Lee<sup>1</sup>Dong-Wook Han<sup>1</sup>

<sup>1</sup>Department of Nanomedical Engineering, BK21 Nano Fusion Technology Division, College of Nanoscience and Nanotechnology, Pusan National University,

<sup>2</sup>Department of Biotechnology Research, National Fisheries Research and Development Institute, Busan,

<sup>3</sup>Electronic Materials Lab, Samsung Corning Precision Materials Co, Ltd, Gumi City, Gyeongsangbukdo, Korea

\*These authors contributed equally to this work

Correspondence: Jaebeom Lee  
Department of Nanomedical Engineering, College of Nanoscience and Nanotechnology, Pusan National University, San 30 Jangjeon-dong, Geumjeong-gu, Busan 609-735, Korea  
Tel +82 55 350 5298  
Fax +82 55 350 5299  
Email jaebeom@pusan.ac.kr

Dong-Wook Han  
Tel +82 55 350 5302  
Fax +82 55 350 5299  
Email nanohan@pusan.ac.kr

**Abstract:** Superparamagnetic iron oxide nanoparticles (SPIONs) have been widely utilized for the diagnosis and therapy of specific diseases, as magnetic resonance imaging (MRI) contrast agents and drug-delivery carriers, due to their easy transportation to targeted areas by an external magnetic field. For such biomedical applications, SPIONs must have multifunctional characteristics, including optimized size and modified surface. However, the biofunctionality and biocompatibility of SPIONs with various surface functional groups of different sizes have yet to be elucidated clearly. Therefore, it is important to carefully monitor the cytotoxicity and genotoxicity of SPIONs that are surfaced-modified with various functional groups of different sizes. In this study, we evaluated SPIONs with diameters of approximately 10 nm and 100~150 nm, containing different surface functional groups. SPIONs were covered with –O– groups, so-called bare SPIONs. Following this, they were modified with three different functional groups – hydroxyl (–OH), carboxylic (–COOH), and amine (–NH<sub>2</sub>) groups – by coating their surfaces with tetraethyl orthosilicate (TEOS), (3-aminopropyl)trimethoxysilane (APTMS), TEOS-APTMS, or citrate, which imparted different surface charges and sizes to the particles. The effects of SPIONs coated with these functional groups on mitochondrial activity, intracellular accumulation of reactive oxygen species, membrane integrity, and DNA stability in L-929 fibroblasts were determined by water-soluble tetrazolium, 2',7'-dichlorodihydrofluorescein, lactate dehydrogenase, and comet assays, respectively. Our toxicological observations suggest that the functional groups and sizes of SPIONs are critical determinants of cellular responses, degrees of cytotoxicity and genotoxicity, and potential mechanisms of toxicity. Nanoparticles with various surface modifications and of different sizes induced slight, but possibly meaningful, changes in cell cytotoxicity and genotoxicity, which would be significantly valuable in further studies of bioconjugation and cell interaction for drug delivery, cell culture, and cancer-targeting applications.

**Keywords:** superparamagnetic iron oxide nanoparticles, surface functional groups, cytotoxicity, genotoxicity

## Introduction

Superparamagnetic iron oxide nanoparticles (SPIONs) have offered attractive possibilities for the improvement of site-specific drug delivery to specific cells, tissues, or even organs<sup>1-3</sup> as well as in the enhancement of magnetic resonance imaging (MRI) contrast,<sup>4-6</sup> hyperthermia treatments,<sup>7-9</sup> and cell and tissue targeting.<sup>10-12</sup> In particular, current advanced techniques in drug targeting use delicate surface modifications for the conjugation of antiangiogenic and anticancer drugs.<sup>13,14</sup> SPIONs have the advantage of easy transportation in vivo to the desired site by an external electrical

magnetic field. Once the external magnetic field is removed, magnetization disappears and the SPIONs remain at the target site for a certain period. This characteristic is unique to SPIONs, which play significant roles in advanced health care systems with a wide range of applications. However, even though SPIONs have already been commercialized in clinical applications, many controversial reports regarding the toxicity of nanoscale materials have been reported, and patient anxiety is still high due to the early adoption of advanced biomedical technologies;<sup>15–17</sup> therefore, an in-depth study on the nanotoxicity of magnetic particles as a drug-carrier system is required.

The size and type of surface functional group are two crucial factors that determine the biological safety of SPIONs, as these factors are known to be directly related to cytotoxicity and genotoxicity, which are pivotal for in vivo practical applications such as drug delivery and targeted imaging.<sup>18</sup> The present study aimed to determine the nanotoxicity and biocompatibility of surface-functionalized SPIONs of different sizes. For this purpose, we used SPIONs with two representative diameters, ie, 10 nm and 100–150 nm, the most commonly issued sizes of nanomaterials, in light of the ambiguous conclusions of recent toxicity studies. For example, a recent study has reported that nanoparticle-mediated cellular response is size-dependent.<sup>19</sup> In contrast, it has been reported that cell recognition in such a small range of size difference might be required for self-cytoprotection.<sup>20,21</sup> Bare SPIONs were modified with three representative functional groups, ie, hydroxyl (–OH), carboxylic (–COOH), and amine (–NH<sub>2</sub>) groups. The toxicity of SPIONs against murine fibroblasts was evaluated by determining changes in cell viability, metabolic activity, oxidative stress, cell membrane integrity, DNA stability, and cell morphology.

## Materials and methods

### Reagents

Iron (II) chloride tetrahydrate (FeCl<sub>2</sub>·4H<sub>2</sub>O, 99%) was purchased from Wako (Osaka, Japan), Iron (III) chloride (FeCl<sub>3</sub>), ammonium hydroxide (NH<sub>4</sub>OH, 28–30 wt%), tetraethyl orthosilicate (TEOS, 99%), (3-aminopropyl) trimethoxysilane (APTMS, >97%), antibiotic antimycotic solution, fetal bovine serum (FBS), and Dulbecco's modified Eagle's medium (DMEM) were obtained from Sigma–Aldrich (St, Louis, MO). Trisodium citrate dehydrates (>99.0%) was purchased from Fluka (Bornem, Belgium). Ethyl alcohol was purchased from Burdick and Jackson (Ulsan, Korea).

## Synthesis of various modified SPIONs

### Synthesis of bare SPIONs

SPIONs were synthesized using Massart's method, based on the coprecipitation of ferrous and ferric ion solutions (1:2 molar ratios).<sup>22</sup> In brief, 5 mL of ammonium hydroxide was added to 10 mmol of FeCl<sub>3</sub> (97%) and 5 mmol of FeCl<sub>2</sub> in 40 mL of distilled water under rapid mechanical stirring at room temperature. Stirring was allowed to continue for 30 minutes, during which a black precipitate was formed. The precipitate was separated by magnetic decantation, washed with 20 mL of ethanol three times, and then air-dried at room temperature. Their diameter was approximately 10 nm with a narrow size distribution. The surface modification of the core SPIONs was immediately carried out to accomplish different sizes and surface functionalities as shown in Table 1.

### Synthesis of TEOS-coated SPIONs

The core/shell SPIONs were synthesized according to the method of Stöber.<sup>23,24</sup> Twenty-five milligrams of SPIONs were redispersed into a mixture of 5 mL ammonium hydroxide, 59.25 mL ethanol, and 25 mL distilled water by sonication. An ethanolic solution of 0.5 mL of TEOS in 10 mL of ethanol was added with mechanical stirring. The hydrolysis and condensation of TEOS onto the SPIONs was completed in 4 hours. These were refined by magnetic precipitation, washed with 20 mL of ethanol three times, and air-dried at room temperature. These core/shell spheres had an average diameter of 100 nm (±10 nm).

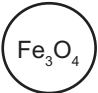

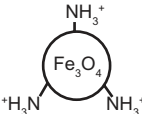
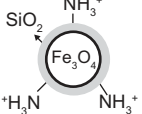
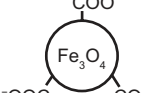
### Synthesis of APTMS-coated SPIONs

The amino-functionalized SPIONs were synthesized according to a previously reported protocol.<sup>25</sup> Twenty-five milligrams of SPIONs were redispersed in 100 mL of distilled water and ethanol mixture (3:7) by sonication. Then, 70 µL of APTMS was added with vigorous stirring and the solution was kept stirring at room temperature overnight. The black precipitate formed was purified by magnetic precipitation, washed with 20 mL of ethanol three times, and air-dried at room temperature.

### Synthesis of TEOS-APTMS (T-A)-coated SPIONs

The same method was used as described in the synthesis of APTMS-coated SPIONs, except that TEOS-coated SPIONs were used instead of bare SPIONs as the initial core material, to prepare SPIONs of a different size with different functional groups. The detailed characteristics and differences between the different SPIONs are schematically described in Table 1.

**Table I** Schematic description of size and surface characteristics of SPIONs tested

Modifying material	Size (nm)	Surface charge (mV)	Surface functional group	Scheme
None (bare)	10	-20	-O <sup>-</sup>	
TEOS	100-150	-30	-O <sup>-</sup>	
APTMS	10	25	-NH <sub>3</sub> <sup>+</sup>	
TEOS-APTMS (T-A)	100-150	30	-NH <sub>3</sub> <sup>+</sup>	
Citrate	10	-40	-COO <sup>-</sup>	

**Abbreviations:** APTMS, (3-aminopropyl)trimethoxysilane; TEOS, tetraethyl orthosilicate.

### Synthesis of citrate-coated SPIONs

Citrate modification was achieved using a popular method already described elsewhere.<sup>26,27</sup> For synthesis of SPIONs, 5 mmol of ferrous and 10 mmol of ferric ion solutions were blended. After adding 5 mL of ammonium hydroxide, stirring was allowed to continue for 10 minutes. The alkaline solution was heated at 90°C and 15 mmol of trisodium citrate was added and then stirred for 30 minutes. The reacted particles were extracted by magnetic force and air-dried at room temperature.

### Physicochemical examinations of SPIONs

The surface potentials of synthesized SPIONs were measured using a Zetasizer (Nano ZS; Malvern Instruments, Worcestershire, UK). The average particle sizes and shapes of SPIONs were determined using transmission electron microscopy (TEM).

### Cell cultures and conditions

A murine fibroblast cell line (L-929 cells from mouse subcutaneous connective tissue) was obtained from the American Type Culture Collection (CCL-1™; ATCC, Rockville, MD). The cells were routinely maintained in DMEM supplemented with 10% FBS and 1% antibiotic antimycotic solution (including 10,000 U penicillin, 10 mg streptomycin, and 25 µg amphotericin B per mL) at 37°C in a humidified atmosphere of 5% CO<sub>2</sub> in air. The cells (1 × 10<sup>5</sup> cells/well)

were seeded in 24-well plates and grown to confluence overnight.

### Cytotoxicity assays

#### WST-8 assay

The number of viable cells was quantified indirectly using highly water-soluble tetrazolium salt (WST-8, 2-(2-methoxy-4-nitrophenyl)-3-(4-nitrophenyl)-5-(2,4-disulfophenyl)-2H-tetrazolium, monosodium salt; Dojindo Lab, Kumamoto, Japan), reduced to a water-soluble formazan dye by mitochondrial dehydrogenases.<sup>28</sup> The cell viability was found to be directly proportional to the metabolic reaction products obtained in WST-8. Briefly, the WST-8 assay was conducted as follows. L-929 cells were treated with increasing concentrations (100-1000 ppm) of each SPION and then incubated with WST-8 for the last 4 hours of the 24 hour culture period at 37°C in the dark. Parallel sets of wells containing freshly cultured nontreated cells were regarded as negative controls. The absorbance was determined at 450 nm using an ELISA reader (SpectraMax® 340; Molecular Device Co, Sunnyvale, CA). The relative cell viability was determined as the percentage ratio of the optical density in the medium (containing SPIONs at each concentration) to that of fresh control medium.

#### DCF assay

The 2',7'-dichlorodihydrofluorescein (DCF) assay is a widely used method to detect intracellular reactive oxygen

species (ROS) levels in pharmacological studies.<sup>29,30</sup> The accumulation of intracellular free radicals from SPIONs was quantified using a ROS assay kit (OxiSelect™; Cell Biolabs, Inc, San Diego, CA), which employs the cell-permeable fluorogenic probe 2',7'-dichlorodihydrofluorescein diacetate (DCFH-DA). DCFH-DA is an ROS detector that can cross cell membranes and be deacetylated by intracellular esterases to nonfluorescent 2',7'-dichlorodihydrofluorescein (DCFH). In the presence of ROS, DCFH is rapidly oxidized to the highly fluorescent DCF, which is readily detectable. The fluorescence intensity is proportional to the ROS levels within the cell cytosol. L-929 cells were exposed to increasing concentrations (200–1000 ppm) of each SPION for 24 hours and then incubated with DCFH-DA for 30 minutes at 37°C in the dark. Parallel sets of wells containing freshly cultured cells were regarded as negative controls. The fluorescence emission of DCF was monitored at regular intervals at an excitation wavelength of 480 nm and an emission wavelength of 530 nm in a fluorescence plate reader (VICTOR<sup>3</sup> Multilabel Counter; PerkinElmer, Inc, Waltham, MA). The amount of DCF formed was calculated from a calibration curve constructed using an authentic DCF standard. The relative DCF fluorescence intensity was calculated as a percentage of the DCF formed in control wells.

### LDH assay

Cell membrane integrity was monitored using a permeability assay to determine the release of lactate dehydrogenase (LDH) into the medium as described previously.<sup>31</sup> The LDH assay (Takara Bio Inc, Shiga, Japan) measures the conversion of a tetrazolium salt into a red formazan product.<sup>32,33</sup> Briefly, after 24 h exposure to increasing concentrations (200–1000 ppm) of each SPION, the supernatant from each well was transferred to a new 96-well plate. Reconstituted substrate mix was added to each well and the plates were kept for 30 minutes in the dark at room temperature. Stop solution was added to each well. Parallel sets of wells containing freshly cultured cells were regarded as negative controls. Released LDH catalyzed the oxidation of lactate to pyruvate with simultaneous reduction of NAD<sup>+</sup> to NADH. The rate of NAD<sup>+</sup> reduction was measured as an increase in absorbance at 340 nm, and was directly proportional to LDH activity in the cell medium. The intensity of red color formed in the assay and measured at a wavelength of 490 nm with an ELISA reader (SpectraMax<sup>®</sup> 340; Molecular Device Co), was proportional to LDH activity and to the number of damaged cells.

### Genotoxicity assay

The comet assay was performed essentially as described by Singh et al,<sup>34</sup> and modified by Da Silva et al.<sup>35</sup> All reagents used were analytical grade (Sigma-Aldrich) unless otherwise stated and the entire process was performed in low light conditions to prevent induced DNA damage. Clear glass slides were precoated with 1% agarose (normal melting point). All slides were shielded from ultraviolet light during preparation and analysis. L-929 cells were exposed to increasing concentrations (200–1000 ppm) of each SPION for 24 hours and then mildly trypsinized. Parallel sets of wells containing freshly cultured cells and 10% dimethyl sulfoxide (DMSO)-treated cells were regarded as negative and positive controls, respectively. An aliquot of the counted cell suspension, sufficient to provide approximately 30,000 cells per gel, was centrifuged (180 × *g*, 5 minutes at 4°C) and the supernatant carefully removed. The cell pellet was then suspended in warm (37°C) 0.6% agarose (low melting point) and two aliquots placed onto a glass slide. Each aliquot was then immediately overlaid with a cover slip. Rapid solidification of the agarose was achieved by placing the slides on a metal tray on ice for 5 minutes. Cover slips were then carefully removed and slides placed in lysis buffer (100 mM EDTA, 2.5 M NaCl, 10 mM Tris–HCl, and 1% Triton X-100, adjusted to pH 10 with NaOH) and left overnight. Following cell lysis, slides were washed twice by submersion in ice-cold deionized water, then transferred to an electrophoresis tank, containing cold electrophoresis buffer (300 mM NaOH and 1 mM EDTA, pH 13) and incubated for 20 minutes to allow unwinding of the DNA. Electrophoresis was carried out for 20 minutes at 30 V and 300 mA. Slides were removed from the tank and flooded with neutralization buffer (0.4 M Tris–HCl, pH 7.5), then rinsed twice with deionized water. The DNA damage was calculated as the percentage of cells with a tail.

### Electron microscopic observations

The morphological alterations of L-929 cells treated with 500 ppm of each SPION were observed by scanning electron microscopy (SEM). In brief, SPION-treated cells were washed with 0.1 M cacodylate buffer (pH 7.4) to remove unattached cells. The cells were fixed with 2.5% glutaraldehyde solution overnight at 4°C, dehydrated with a series of increasing concentration of ethanol solution, and then vacuum-dried. The fixed cell cultures were coated with an ultra-thin layer of gold/platinum by an ion sputter (E1010; Hitachi, Tokyo, Japan), and then observed under a SEM (Hitachi S-800) at an accelerating voltage of 20 kV.



TEM was also performed to obtain information regarding the intracellular ultrastructure and distribution of SPIONs penetrated into cells. After treatment with each SPION for 24 hours, the cells were immediately fixed with 2% glutaraldehyde, rinsed with phosphate-buffered saline (PBS, pH 7.4), and then post-fixed in 1% sodium cacodylate-buffered osmium tetroxide ( $\text{OsO}_4$ ). The fixed cell cultures were subsequently dehydrated through a graded series of ethanol solutions and finally embedded in situ by covering with a layer of Spurr epoxy resin (Polysciences Inc, Warrington, PA), which was allowed to polymerize. Prepared blocks were sectioned using a diamond knife mounted in a Reichert ultracut microtome (Leica, Heidelberg, Germany). Ultrathin sections (70–80 nm) were contrasted with uranyl acetate and lead citrate, and observed using an electron microscope (CM-120; Philips, Eindhoven, Netherlands) at 80 kEv.

## Statistical analyses

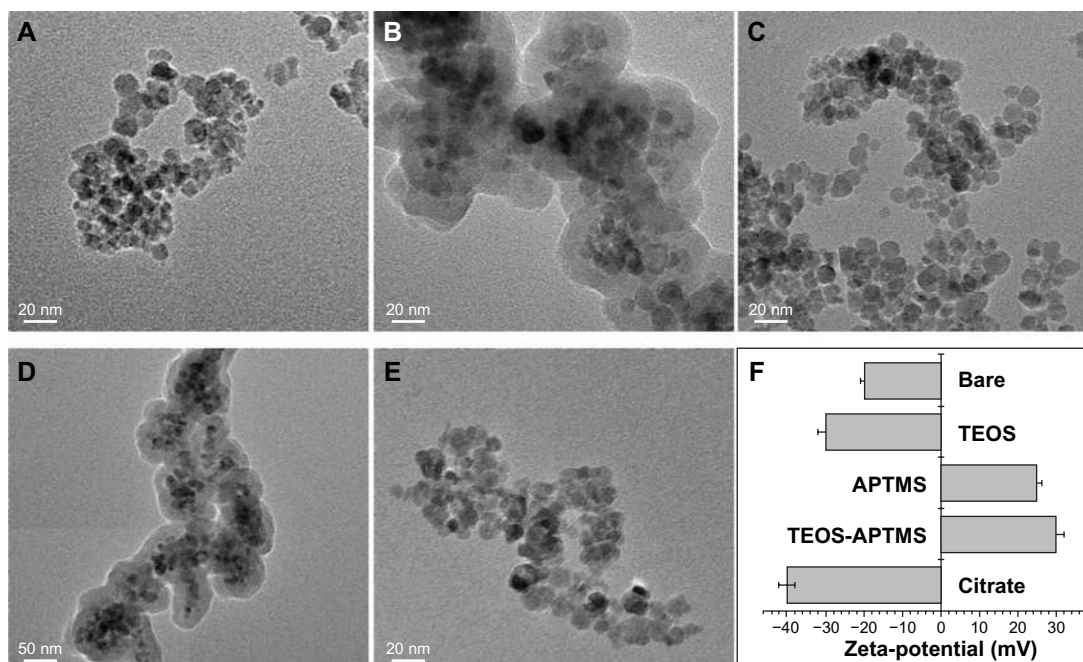
All variables were tested in three independent cultures for cytotoxicity assays and genotoxicity assay, and each assay was repeated twice ( $n = 6$ ). The cytotoxicity results are reported as the mean  $\pm$  standard deviation (SD) compared with the nontreated controls. The genotoxicity result is reported as the content (%) of cells with tail DNA. A one-way analysis of

variance (ANOVA), which was followed by a Tukey honestly significant difference test for the multiple comparisons, was used to detect the dose-dependent effects of various SPIONs on L-929 cells. A  $P$ -value  $< 0.05$  was considered statistically significant.

## Results and discussion

### Spectroscopic and microscopic analysis of SPIONs with different functional groups

We synthesized SPIONs with an average diameter of 10 nm (Table 1) – so-called bare SPIONs (Figure 1A). All subsequent surface and size modifications were initiated from these nanoparticles. Figure 1A, C, and E represent electron microscopic images of the different functional groups of SPIONs without the  $\text{SiO}_2$  shell, whereas Figure 1B and D show SPIONs with  $\text{SiO}_2$  shells. The core SPIONs were mostly similar in size, because the nucleation and growth conditions of nanoparticle synthesis were identical. Following this, a surface modification process was carried out using various functional groups, resulting in the formation of a single layer of functional groups on the nanoparticle. The core materials in Figure 1B and D consisted of 4–5 SPIONs, and the thickness of the  $\text{SiO}_2$  shell was easily adjusted by altering TEOS molarity. The core/shell structure used in the nanotoxicity experiment had a core



**Figure 1** Physicochemical characterization of SPIONs tested. TEM images of bare SPIONs (A) and SPIONs modified with TEOS (B), APTMS (C), TEOS-APTMS (D), or citrate (E), along with the zeta-potentials (F) of each SPION.

**Note:** The TEM images shown in this figure are representative of six independent experiments with similar results.

**Abbreviations:** APTMS, (3-aminopropyl)trimethoxysilane; SPION, superparamagnetic iron oxide nanoparticles; TEM, transmission electron microscopy; TEOS, tetraethyl orthosilicate.

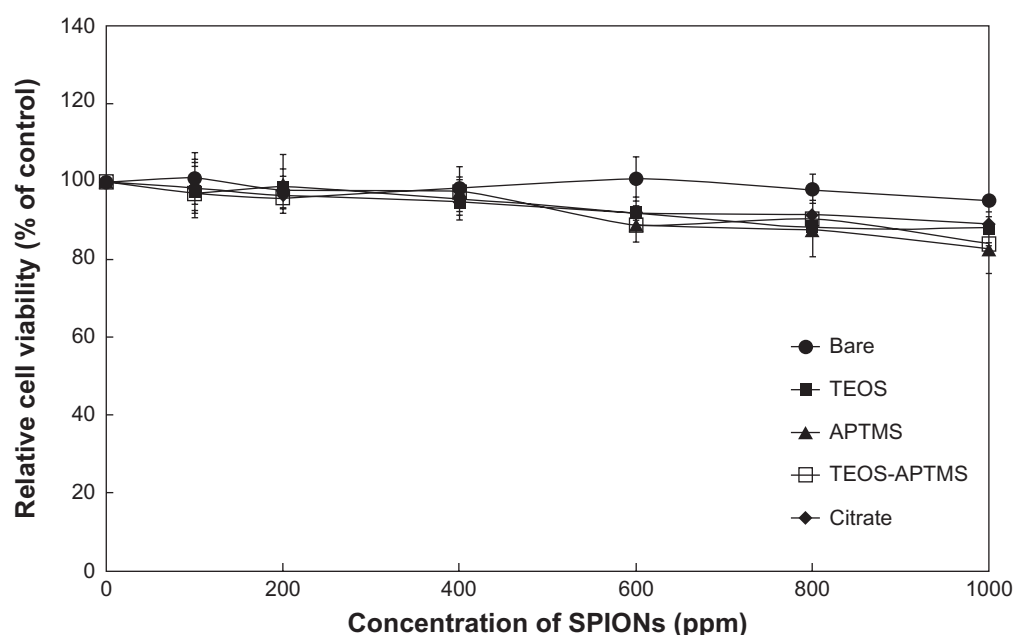
diameter of approximately 40 nm and an average  $\text{SiO}_2$  shell thickness of 60 nm, yielding an average total diameter of 100–150 nm. The functional groups were amine or carboxylic groups, which may yield strong positive and negative potentials due to ionization in solution. When the surfaces of the SPIONs were modified by these strong charged chemical groups, the differently functionalized SPIONs were dispersed well in PBS due to the high repulsion forces among the nanoparticles. Because of the magnetic property of the SPIONs, they were observed aggregately in the TEM grid surface. However, the nanoparticles were mostly well-dispersed due to strong charge–charge repulsion among nanoparticles. Zeta-potential analysis of surface potentials shows that all the SPIONs were charged at over  $\pm 20$  mV, which is sufficient to be repulsive in neutral solvent (Figure 1F). From the Zetasizer histograms for the size distributions of the SPIONs, it was confirmed that the particles were separated in aqueous solution (Supplementary Figure S1). Relatively small SPIONs (ie, bare and APTMS- or citrate-coated) showed an average diameter of 10 nm and large SPIONs (ie, TEOS- or T-A-coated) showed an average diameter of 150 nm.

## Cytotoxicity of SPIONs coated with various functional groups

### Effects of SPIONs on cell viability

L-929 cells were treated with each SPION and cytotoxicity was measured using a WST-8 assay.<sup>36</sup> Once SPIONs were

air-dried, their solubility decreased. At concentrations above 1000 ppm, the solution was saturated and additional particles were easily precipitated. Therefore, 1000 ppm was determined as the upper limit of concentration for sample preparation. Figure 2 presents the results of the WST-8 assay. A dose-dependent reduction was observed in WST-8 absorbance in cells treated with increasing concentrations (100–1000 ppm) of each SPION for 24 hours. The different SPIONs caused no significant reduction in cell viability at lower concentrations but induced substantial reductions at concentrations above 400 ppm. At the highest concentration (1000 ppm), we observed a ~15% loss of cell viability, except in the case of the bare SPIONs. At concentrations below 200 ppm, the various modified SPIONs showed no cytotoxic effects on cells and the cells remained more than 85% viable relative to the control. Our observations suggest that SPION concentration is more critical than any other factor, such as surface modification or size. Based on *in vitro* cytotoxicity, it can be concluded that SPIONs can be used in bioapplications at concentrations below 500 ppm, determined as conservatively as possible. However, the WST-8 assay evaluates cytotoxicity based only on the activity of mitochondrial dehydrogenases; therefore, the possibility still remains that toxicity in cells exposed to SPIONs might result from interference with signaling cascades related to cell survival.



**Figure 2** Effect of SPIONs on mitochondrial activity. Relative cell viability of L-929 cells exposed for 24 hours to increasing concentrations (0–1000 ppm) of SPIONs coated with various functional groups was evaluated using the WST-8 assay.

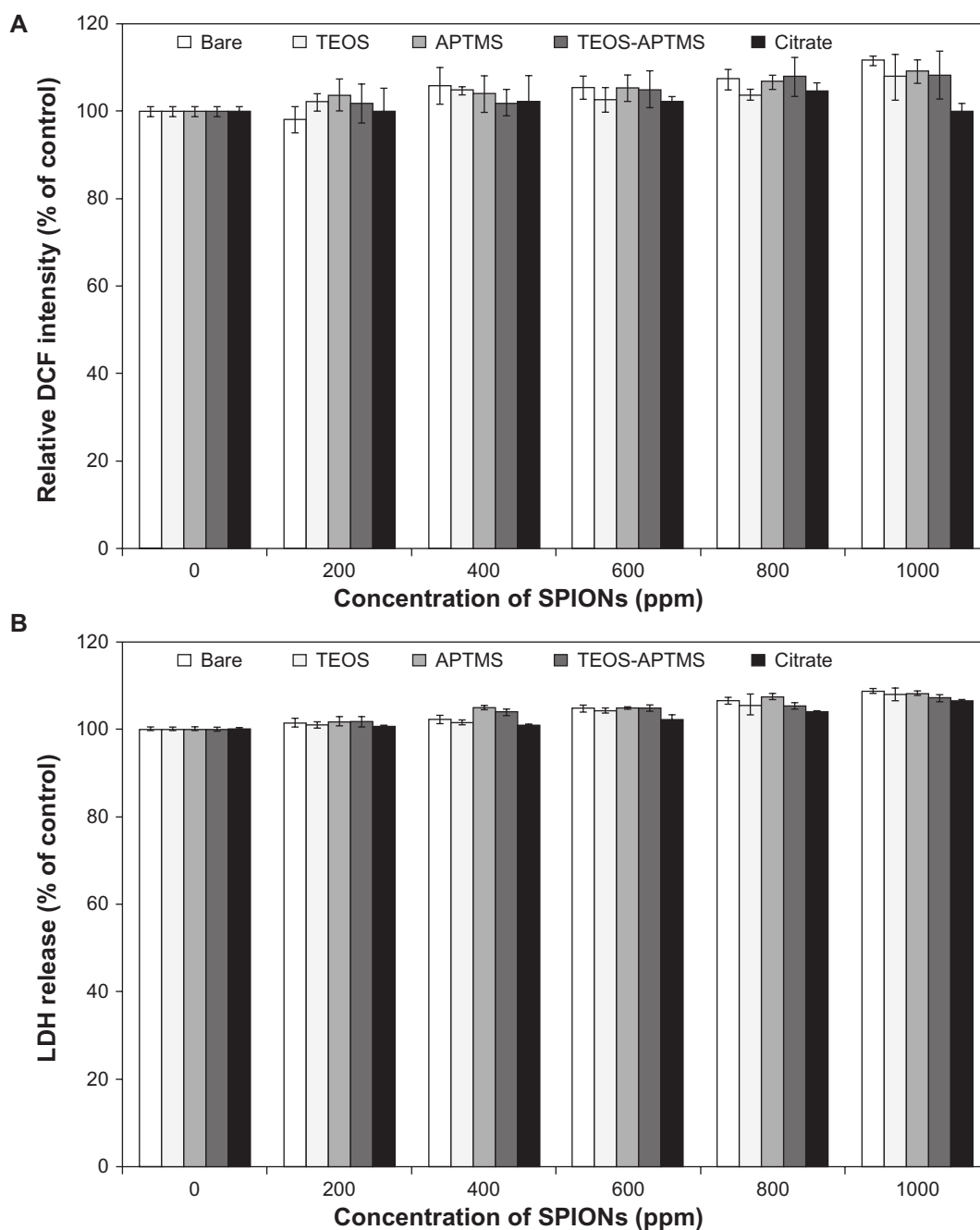
**Abbreviations:** APTMS, (3-aminopropyl)trimethoxysilane; SPION, superparamagnetic iron oxide nanoparticles; TEOS, tetraethyl orthosilicate.

## Effects of SPIONs on oxidative stress and cell membrane integrity

The DCF assay has been well verified as an effective index for evaluating the toxicity of nanomaterials attributable to ROS generation.<sup>37,38</sup> We used modified SPIONs and observed the state of oxidative stress in cells after 24 hours of exposure to each material at five concentrations in the range from 200 to 1000 ppm. As shown in Figure 3A, the ROS generation

increased in a dose-dependent manner as the concentration of SPIONs increased, with the exception of SPIONs containing citrate. However, the results did not correlate exactly with the cell viability data, suggesting that toxicity in cells exposed to SPIONs might be attributed to another mechanism.

LDH leakage is well known as a useful index for cytotoxicity on the basis of loss of membrane integrity. All the SPIONs induced apparent LDH leakage from L-929 cells



**Figure 3** Effects of SPIONs on oxidative stress and cell membrane integrity. Intracellular ROS levels (A) and LDH release profiles (B) in L-929 cells exposed to increasing concentrations (0–1000 ppm) of SPIONs coated with various functional groups for 24 hours were evaluated by the DCF and LDH assays, respectively.

**Abbreviations:** APTMS, (3-aminopropyl)trimethoxysilane; DCF, 2,2'-dichlorodihydrofluorescein; LDH, lactate dehydrogenase; ROS, reactive oxygen species; SPION, superparamagnetic iron oxide nanoparticles; TEOS, tetraethyl orthosilicate.

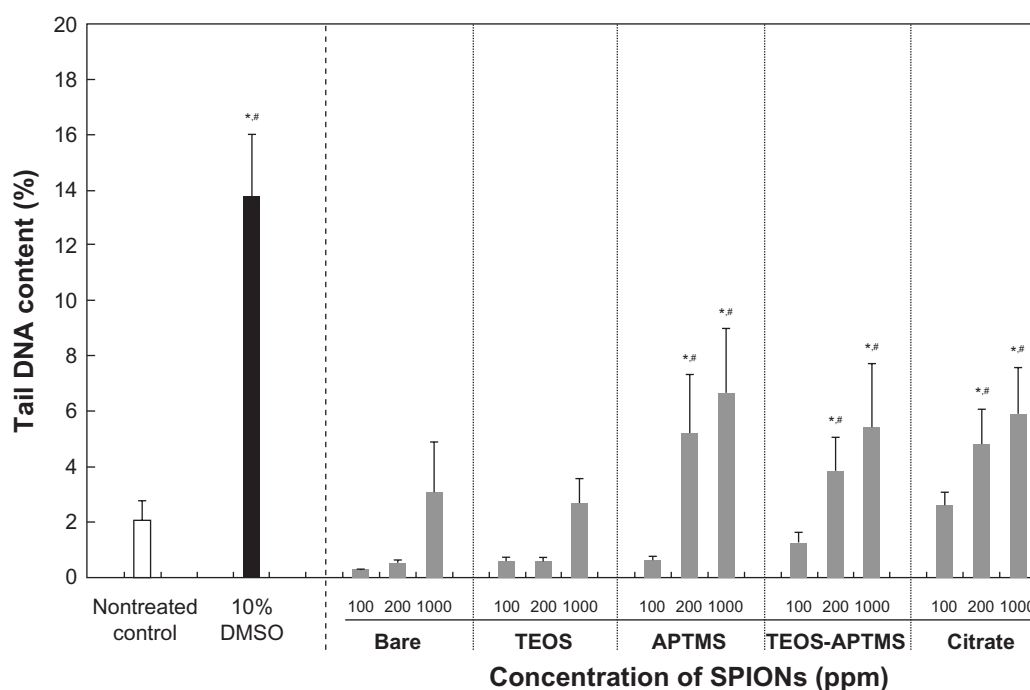
treated for 24 hours, revealing the impact of SPIONs on cell membrane integrity (Figure 3B). LDH levels in the cell medium showed a slight increase with increasing particle concentrations. Following exposure at the highest dose (1000 ppm), LDH release was about 108% of that seen in untreated control. However, there were no significant differences in cellular viability when comparing the effects of different types of SPIONs at the same dose. In contrast with the results of the WST-8 and DCF assays, there was no consistent evidence of cytotoxicity at all. Therefore, we suggest that acute cytotoxicity might primarily originate from the cellular internalization of nanoparticles, rather than physical damage to the cellular membrane.

## Genotoxicity of SPIONs coated with various functional groups

A comet assay of SPION-treated cells showed a concentration-dependent increase in tail momentum compared to control cells, indicating the presence of DNA damage (Figure 4). L-929 cells were treated with SPION concentrations of 100, 200, and 1000 ppm, and DMSO was used as a positive control. No extensive and dose-dependent damage to DNA was observed after treatment of the cells with bare and TEOS-coated SPIONs. The tail DNA contents in bare and TEOS-modified SPIONs were shown to be lower than

3% even at a concentration of 1000 ppm. When the highest concentration was added, the genotoxicity of both particles rapidly increased and slightly exceeded that seen with the negative control (vehicle); however, the observed genotoxicity was still less than that seen with DMSO treatment. These results are well correlated with the trends seen in the WST-8 assay in Figure 2. In contrast, the SPIONs modified with APTMS and T-A showed dose-dependent genotoxic effects on the cells, suggesting that these positively charged particles enter into the nucleus through the nuclear pore and interact directly with the DNA, which is negatively charged due to its phosphate groups.

Interestingly, the cells treated with 200 ppm of citrate-modified SPION showed a significant difference compared with those treated with the same dose of bare and TEOS-coated SPIONs. This phenomenon may be explained partly by the fact that citrate-modified SPIONs penetrated through nuclear membrane generated highly reactive hydroxyl radicals, leading to DNA attack. Citrate is a commonly used stabilizer in the synthesis of various particles.<sup>39,40</sup> The chemical reactions that bring about such mutations are based on the formation of the highly reactive and short-lived hydroxyl radical ( $\text{OH}^\bullet$ ) in close proximity to DNA.<sup>41</sup> This citrate-mediated damage might also be associated with a specific cell signaling pathway or an unexpected experimental factor;



**Figure 4** Effects of SPIONs on DNA stability. Tail content of DNA in L-929 cells exposed to increasing concentrations (0–1000 ppm) of SPIONs coated with various functional groups for 24 hours was determined by the comet assay.

**Notes:** \* $P < 0.05$  vs nontreated control; # $P < 0.05$  vs SPION-treated cells with 100 ppm.

**Abbreviations:** APTMS, (3-aminopropyl)trimethoxysilane; DMSO, dimethyl sulfoxide; SPION, superparamagnetic iron oxide nanoparticles; TEOS, tetraethyl orthosilicate.



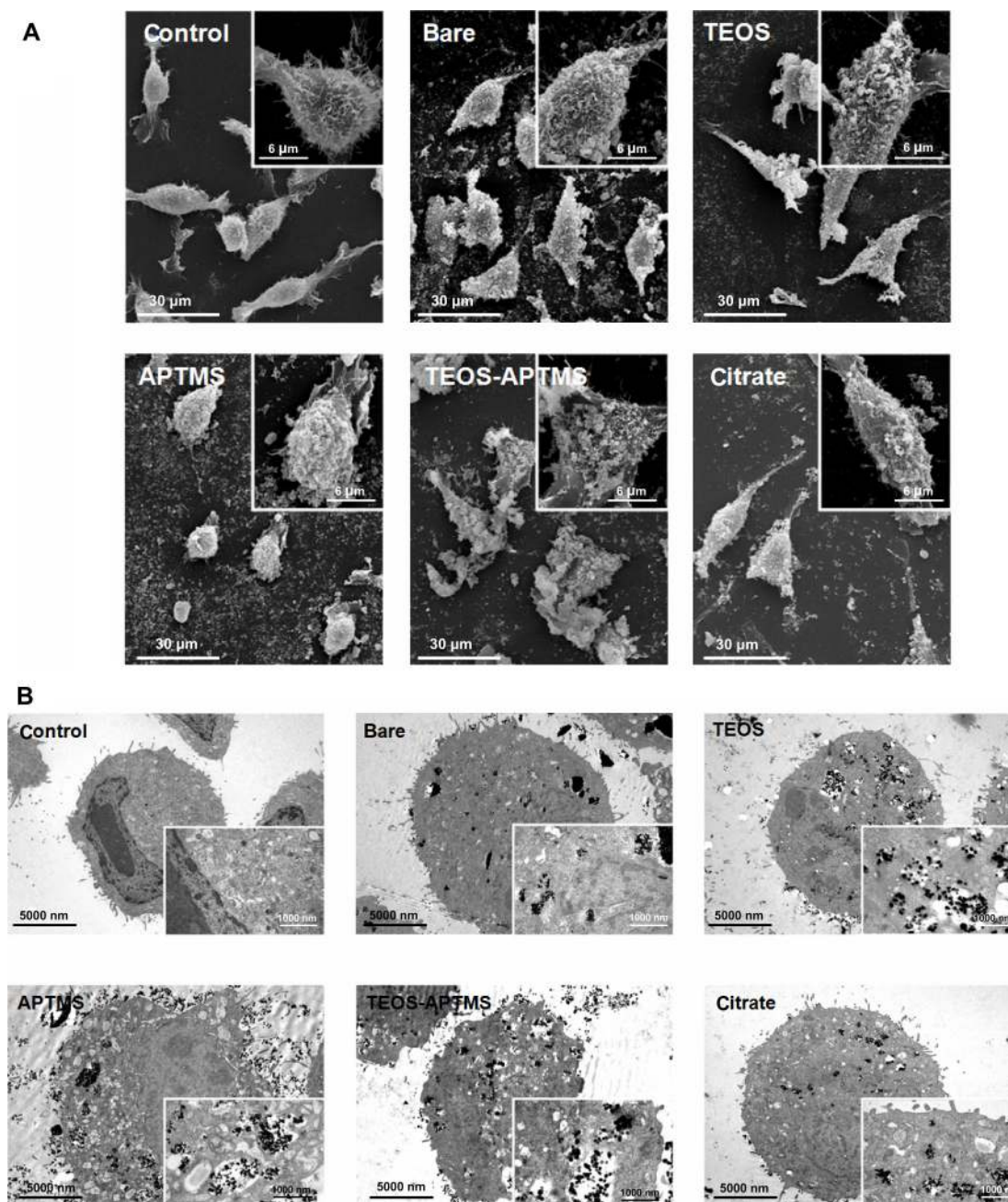
therefore, it is difficult to analyze toxicity resulting from the damage to DNA. The genotoxic mechanism may be revealed from further consecutive experiments. It is generally noted from the experimental data that the higher the SPION concentration, the lower the cell viability and the worse the genotoxicity. Based on the results of the genotoxicity assay, we also predict that the toxicity of SPIONs might result in DNA damage via magnetic oxidation of the SPIONs. It has been reported that SPIONs may cause low levels of toxicity (evaluated by the comet assay) due to their potency in causing oxidative DNA lesions in cultured A549 cells (the human lung epithelial cell line).<sup>42</sup> Our results indicate that SPIONs rarely show genotoxicity below 100 ppm, but more careful investigation is required when SPIONs are treated at concentrations above 200 ppm. Based on these observations, we may validate the commercial use of SPIONs in clinics based on our experimental results even though a direct comparison may not be available. For clinical labeling of cells in MRI, commercialized SPIONs (Resovist®, Schering, Germany) have been used at concentrations of 5–25 ppm ( $\mu\text{g/mL}$ ) depending on the patient's weight;<sup>43,44</sup> this concentration range is biologically safe based on our data from Figures 2 and 4.

## SEM and TEM observations

SEM and TEM images of each cell were obtained after the cytotoxicity test. Figure 5A shows the SEM images of L-929 cells treated with each SPION at a concentration of 500 ppm; the WST-8 assay indicates that the cells might be partly damaged at this concentration. SEM micrographs allow the observation of the surface of SPION-adhered cells. The cell membrane consists of a phospholipid bilayer, which is repulsive to charged materials, so that we may observe different tomographic images depending on the surface charge of the nanoparticles. It was found that the aggregates of SPIONs were attached to the cell surface even though the surface charges of each SPION were over  $\pm 20$  mV. It is not clear which step was originated between aggregation of SPIONs or attachment on cell surface. The stability of nanoparticles in the cell culture medium may be one of the most crucial factors in evaluating toxicity and further understanding the toxicity mechanism. In several reports by using materials similar to our study,<sup>45,46</sup> SPIONs were shown to be stable below 1000 ppm in aqueous solution. All SPIONs here were well dispersed in aqueous solution even at 1000 ppm as they had been sufficiently sonicated. Over 1000 ppm, particles were started to saturate and precipitate even though sonication was given. Positively charged SPIONs (ie, APTMS- and

T-A-modified) appear to be firmly attached to the cell surface, compared with the other negatively charged nanoparticles. This observation can be explained by the fact that the resting membrane potential of cells is negative. We suggest that the negatively charged membrane preferentially attracts positively charged, rather than negatively charged particles. With increasing concentrations, the number of attached SPIONs proportionally increased (data not shown). Surprisingly, the LDH results shown in Figure 3B indicate that these attached particles had no effect on cell viability, implying that SPIONs rarely affected cell membrane integrity. However, it is possible that they act via different pathways, as mechanisms of uptake are very complex. The nanoparticles might penetrate into the cell via endocytotic mechanisms such as phagocytosis, pinocytosis, nonspecific endocytosis, receptor-mediated endocytosis, etc.<sup>47,48</sup>

TEM studies were also performed to track a detailed cellular uptake of SPIONs (Figure 5B). The internalization of SPIONs is highly related to their coating material, shape, and size. Compared with the nontreated control cells, there was a substantial increase in the amount of SPION inside the cell. From TEM images, it was revealed that the positively charged SPIONs (APTMS and T-A-coated) seemed to be more concentrated inside the cell than the negatively charged SPIONs (bare, TEOS- and citrate-coated). Moreover, the integrity of cell membrane was shown to be more severely damaged with intracellular vesicles containing more concentrated SPIONs in the cell exposed to APTMS- and T-A-coated SPIONs. This observation correlates well with the SEM observations, which show that the positively charged SPIONs attached preferentially to the cell surface. It might be concluded that positively charged nanoparticles are more likely to be attracted to the cell membrane, which is negatively charged in solution. Although the charge–charge interaction may be helpful to increase the accessibility of SPIONs to the cell membrane, our present results, as well as many other studies, indicate that larger nanoparticles (100–150 nm) would penetrate the cell membrane more easily by endocytosis than smaller nanoparticles ( $\sim 10$  nm).<sup>49–51</sup> Cell toxicity may therefore be elucidated based on these results. However, the observed cytotoxicity did not match well with SPION endocytosis observed by SEM and TEM, because all SPIONs showed similar cytotoxicity regardless of their tendency to internalize. Furthermore, in genotoxicity analysis, the negatively charged (ie, citrate-modified) SPION presented the highest toxicity at low concentrations (100 ppm). Above 100 ppm, the tendency towards genotoxicity was similar regardless of the size and surface charge but the change was



**Figure 5** Electron microscopy images of L-929 cells. Morphological alterations and intracellular ultrastructures of L-929 cells exposed to 500 ppm of SPIONs coated with various functional groups for 24 hours were observed by SEM (A) and TEM (B), respectively.

**Notes:** The scale bars in the large and inserted SEM images were 30 µm and 6 µm, respectively. The scale bars in the large and inserted TEM images were 5000 nm and 1000 nm, respectively. The electron micrographs shown in this figure are representative of six independent experiments with similar results.

**Abbreviations:** APTMS, (3-aminopropyl)trimethoxysilane; DMSO, dimethyl sulfoxide; SEM, scanning electron microscopy; SPION, superparamagnetic iron oxide nanoparticles; TEM, transmission electron microscopy; TEOS, tetraethyl orthosilicate.

not significant. From these results, we observed a detailed dependence of cell cytotoxicity and genotoxicity on the surface modification and size of nanoparticles. It is obvious that small modifications in these nanoparticles induced slight but possibly meaningful changes in cell cytotoxicity and genotoxicity; this information would be significantly valuable in studies of bio-conjugation and cell interaction for drug

delivery, cell culture, cancer-targeting applications or further advanced precise control-required bioengineering.

## Conclusion

We observed that SPIONs affected the cell viability and DNA stability of L-929 fibroblastic cells in a dose-dependent manner. In the macroscopic view of the cell itself, SPIONs

appear not to be cytotoxic and genotoxic to fibroblastic cells at concentrations lower than 500 ppm. However, it was obvious that the small modification of the nanoparticles induced subtle variations in their cellular internalization, or endocytosis. Furthermore, noticeable differences in the genotoxicity of different SPIONs, possibly due to variations in size and charge, were observed at low concentrations.

## Acknowledgment

This work was supported by the Bio-Scientific Research Grant funded by the Pusan National University (PNU, Bio-Scientific Research Grant; PNU-2008-101-20080608000).

## Disclosure

The authors report no conflicts of interest in this work.

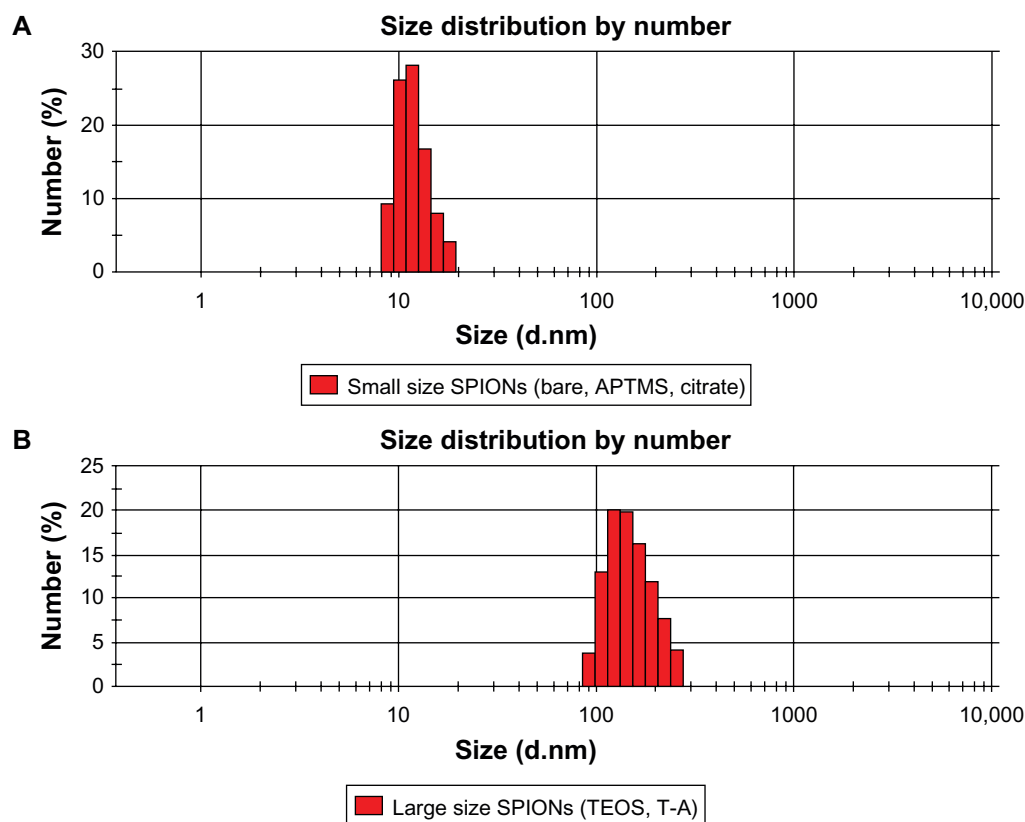
## References

- Arruebo M, Fernandez-Pacheco R, Ibarra MR, Santamaria J. Magnetic nanoparticles for drug delivery. *Nano Today*. 2007;2(3):22–32.
- McBain SC, Yiu HH, Dobson J. Magnetic nanoparticles for gene and drug delivery. *Int J Nanomedicine*. 2008;3(2):169–180.
- Kim J, Lee JE, Lee SH, et al. Designed fabrication of a multifunctional polymer nanomedical platform for simultaneous cancer-targeted imaging and magnetically guided drug delivery. *Adv Mater*. 2008;20(3):478–483.
- Park SI, Kwon BJ, Park JH, et al. Synthesis and characterization of 3-[131I] iodo-L-tyrosine grafted  $\text{Fe}_3\text{O}_4/\text{SiO}_2$  nanocomposite for single photon emission computed tomography (SPECT) and magnetic resonance imaging (MRI). *J Nanosci Nanotechnol*. 2011;11(2):1818–1821.
- Sosnovik DE, Nahrendorf M, Weissleder R. Magnetic nanoparticles for MR imaging: agents, techniques and cardiovascular applications. *Basic Res Cardiol*. 2008;103(2):122–130.
- Hong RY, Feng B, Chen LL, et al. Synthesis, characterization and MRI application of dextran-coated  $\text{Fe}_3\text{O}_4$  magnetic nanoparticles. *Biochem Eng J*. 2008;42(3):290–300.
- Reena Mary AP, Narayanan TN, Sunny V, et al. Synthesis of bio-compatible spion-based aqueous ferrofluids and evaluation of radiofrequency power loss for magnetic hyperthermia. *Nanoscale Res Lett*. 2010;5(10):1706–1711.
- Tseng HY, Lee GB, Lee CY, Shih YH, Lin XZ. Localised heating of tumours utilising injectable magnetic nanoparticles for hyperthermia cancer therapy. *IET Nanobiotechnol*. 2009;3(2):46–54.
- Shi D, Cho HS, Chen Y, et al. Fluorescent polystyrene- $\text{Fe}_3\text{O}_4$  composite nanospheres for in vivo imaging and hyperthermia. *Adv Mater*. 2009;21(21):2170–2173.
- Lee WY, Cheng WY, Yeh YC, et al. Magnetically directed self-assembly of electrospun superparamagnetic fibrous bundles to form three-dimensional tissues with a highly ordered architecture. *Tissue Eng Part C: Methods*. 2011;17(6):651–661.
- Xu C, Xie J, Ho D, et al. Au- $\text{Fe}_3\text{O}_4$  dumbbell nanoparticles as dual-functional probes. *Angew Chem Int Edit*. 2008;47(1):173–176.
- Yang X, Chen Y, Yuan R, et al. Folate-encoded and  $\text{Fe}_3\text{O}_4$ -loaded polymeric micelles for dual targeting of cancer cells. *Polymer*. 2008;49(16):3477–3485.
- Xing R, Wang X, Zhang C, et al. Superparamagnetic magnetite nanocrystal clusters as potential magnetic carriers for the delivery of platinum anticancer drugs. *J Mater Chem*. 2011;21(30):11142–11149.
- Lin BL, Shen XD, Cui S. Application of nanosized  $\text{Fe}_3\text{O}_4$  in anticancer drug carriers with target-orientation and sustained-release properties. *Biomed Mater*. 2007;2(2):132–134.
- Shubayev VI, Pisanic TR II, Jin S. Magnetic nanoparticles for theragnostics. *Adv Drug Deliv Rev*. 2009;61(6):467–477.
- Laurent S, Forge D, Port M, et al. Magnetic iron oxide nanoparticles: Synthesis, stabilization, vectorization, physicochemical characterizations, and biological applications. *Chem Rev*. 2008;108(6):2064–2110.
- Mou Y, Chen B, Zhang Y, et al. Influence of synthetic superparamagnetic iron oxide on dendritic cells. *Int J Nanomedicine*. 2011;6:1779–1786.
- Schlachter EK, Widmer HR, Bregy A, et al. Metabolic pathway and distribution of superparamagnetic iron oxide nanoparticles: in vivo study. *Int J Nanomedicine*. 2011;6:1793–1800.
- Jiang W, Kim BY, Rutka JT, Chan WC. Nanoparticle-mediated cellular response is size-dependent. *Nat Nanotechnol*. 2008;3(3):145–150.
- Zauner W, Farrow NA, Haines AMR. In vitro uptake of polystyrene microspheres: effect of particle size, cell line and cell density. *J Control Release*. 2001;71(1):39–51.
- Chithrani BD, Ghazani AA, Chan WC. Determining the size and shape dependence of gold nanoparticle uptake into mammalian cells. *Nano Lett*. 2006;6(4):662–668.
- Massart R. Preparation of aqueous magnetic liquids in alkaline and acidic media. *IEEE T Magn*. 1981;17(2):1247–1248.
- Stober W, Fink A, Bohn E. Controlled growth of monodisperse silica spheres in the micron size range. *J Colloid Interf Sci*. 1968;26(1):62–69.
- Salgueirino-Maceira V, Correa-Duarte MA, Spasova M, Liz-Marzán LM, Farle M. Composite silica spheres with magnetic and luminescent functionalities. *Adv Funct Mater*. 2006;16(10):509–514.
- Rossi LM, Quach AD, Rosenzweig Z. Glucose oxidase-magnetite nanoparticle bioconjugate for glucose sensing. *Anal Bioanal Chem*. 2004;380(4):606–613.
- Sauzedde F, Elaissari A, Pichot C. Hydrophilic magnetic polymer latexes. 1. Adsorption of magnetic iron oxide nanoparticles onto various cationic latexes. *Colloid Polym Sci*. 1999;277(9):846–855.
- Hong RY, Li JH, Zhang SZ, et al. Preparation and characterization of silica-coated  $\text{Fe}_3\text{O}_4$  nanoparticles used as precursor of ferrofluids. *Appl Surf Sci*. 2009;255(6):3485–3492.
- Wang C, Zhang H, Chen B, Yin H, Wang W. Study of the enhanced anticancer efficacy of gambogic acid on Capan-1 pancreatic cancer cells when mediated via magnetic  $\text{Fe}_3\text{O}_4$  nanoparticles. *Int J Nanomedicine*. 2011;6:1929–1935.
- Mattson MP, Barger SW, Begley JG, Mark RJ. Calcium, free radicals, and excitotoxic neuronal death in primary cell culture. *Methods Cell Biol*. 1995;46:187–216.
- Maxwell DP, Wang Y, McIntosh L. The alternative oxidase lowers mitochondrial reactive oxygen production in plant cells. *Proc Natl Acad Sci U S A*. 1999;96(14):8271–8276.
- Scott GS, Virag L, Szabo C, Hooper DC. Peroxynitrite induced oligodendrocyte toxicity is not dependent on poly(ADP-ribose) polymerase activation. *Glia*. 2003;41(2):105–116.
- Nie BM, Yang LM, Fu SL, Jiang XY, Lu PH, Lu Y. Protective effect of panaxydol and panaxynol on sodium nitroprusside-induced apoptosis in cortical neurons. *Chem Biol Interact*. 2006;160(3):225–231.
- Issa Y, Watts DC, Brunton PA, Waters CM, Duxbury AJ. Resin composite monomers alter MTT and LDH activity of human gingival fibroblasts in vitro. *Dent Mater*. 2004;20(1):12–20.
- Singh NP, McCoy MT, Tice RR, Schneider EL. A simple technique for quantitation of low levels of DNA damage in individual cells. *Exp Cell Res*. 1988;175(1):184–191.
- Da Silva FR, Erdtmann B, Dalpiaz T, et al. Effects of dermal exposure to nicotiana tabacum (Jean Nicot, 1560) leaves in mouse evaluated by multiple methods and tissues. *J Agric Food Chem*. 2010;58(17):9868–9874.
- Jiang Z, Chen BA, Xia GH, et al. The reversal effect of magnetic  $\text{Fe}_3\text{O}_4$  nanoparticles loaded with cisplatin on SKOV3/DDP ovarian carcinoma cells. *Int J Nanomedicine*. 2009;4:107–114.
- Xia T, Kovochich M, Brant J, et al. Comparison of the abilities of ambient and manufactured nanoparticles to induce cellular toxicity according to an oxidative stress paradigm. *Nano Lett*. 2006;6(8):1794–1807.

38. Guo B, Zebda R, Drake SJ, Sayes CM. Synergistic effect of co-exposure to carbon black and Fe<sub>2</sub>O<sub>3</sub> nanoparticles on oxidative stress in cultured lung epithelial cells. *Part Fibre Toxicol.* 2009;6:4.
39. Jin R, Charles Cao Y, Hao E, Métraux GS, Schatz GC, Mirkin CA. Controlling anisotropic nanoparticle growth through plasmon excitation. *Nature.* 2003;425(6957):487–490.
40. Jana NR, Gearheart L, Murphy CJ. Seeding growth for size control of 5–40 nm diameter gold nanoparticles. *Langmuir.* 2001;17(22):6782–6786.
41. Cadet J, Delatour T, Douki T, et al. Hydroxyl radicals and DNA base damage. *Mutat Res.* 1999;424(1–2):9–21.
42. Karlsson HL, Cronholm P, Gustafsson J, Möller L. Copper oxide nanoparticles are highly toxic: A comparison between metal oxide nanoparticles and carbon nanotubes. *Chem Res Toxicol.* 2008;21(9):1726–1732.
43. Guo J, Shen JK, Wang L, et al. In vivo evaluation of cerebral transplantation of resovist-labeled bone marrow stromal cells in Parkinson's disease rats using magnetic resonance imaging. *Appl Biochem Biotechnol.* 2011;163(5):636–648.
44. Park KS, Lee HS, Kim YS, et al. Improved quantification of islet transplants by magnetic resonance imaging with Resovist. *Pancreas.* 2011;40(6):911–919.
45. Mahmoudi M, Simchi A, Milani AS, Stroeve P. Cell toxicity of superparamagnetic iron oxide nanoparticles. *J Colloid Interface Sci.* 2009;336(2):510–518.
46. Mahmoudi M, Laurent S, Shokrgozar MA, Hosseinkhani M. Toxicity evaluations of superparamagnetic iron oxide nanoparticles: cell “vision” versus physicochemical properties of nanoparticles. *ACS Nano.* 2011;5(9):7263–7276.
47. Lee J, Kim HY, Zhou H, et al. Green synthesis of phytochemical-stabilized Au nanoparticles under ambient conditions and their biocompatibility and antioxidative activity. *J Mater Chem.* 2011;21(35):13316–13326.
48. Sohaebuddin SK, Thevenot PT, Baker D, Eaton JW, Tang L. Nanomaterial cytotoxicity is composition, size, and cell type dependent. *Part Fibre Toxicol.* 2010;7:22.
49. Win KY, Feng SS. Effects of particle size and surface coating on cellular uptake of polymeric nanoparticles for oral delivery of anticancer drugs. *Biomaterials.* 2005;26(15):2713–2722.
50. Desai MP, Labhasetwar V, Amidon GL, Levy RJ. Gastrointestinal uptake of biodegradable microparticles: effect of particle size. *Pharm Res.* 1996;13(12):1838–1845.
51. Conner SD, Schmid SL. Regulated portals of entry into the cell. *Nature.* 2003;422(6927):37–44.



## Supplementary figure



**Figure S1** Size distributions of relatively small SPIONs (ie, bare and APTMS- or citrate-coated) (**A**) and large SPIONs (ie, TEOS- or T-A-coated) (**B**) in aqueous solution.

**Note:** The Zetasizer histograms shown in this figure are representative of five independent experiments with almost similar results.

**Abbreviations:** APTMS, (3-aminopropyl)trimethoxysilane; DMSO, dimethyl sulfoxide; SPION, superparamagnetic iron oxide nanoparticles; T-A, TEOS-APTMS; TEOS, tetraethyl orthosilicate.

International Journal of Nanomedicine

**Publish your work in this journal**

The International Journal of Nanomedicine is an international, peer-reviewed journal focusing on the application of nanotechnology in diagnostics, therapeutics, and drug delivery systems throughout the biomedical field. This journal is indexed on PubMed Central, MedLine, CAS, SciSearch®, Current Contents®/Clinical Medicine,

Submit your manuscript here: <http://www.dovepress.com/international-journal-of-nanomedicine-journal>

Journal Citation Reports/Science Edition, EMBase, Scopus and the Elsevier Bibliographic databases. The manuscript management system is completely online and includes a very quick and fair peer-review system, which is all easy to use. Visit <http://www.dovepress.com/testimonials.php> to read real quotes from published authors.

Dovepress